Weakly-bound projectiles in heavy targets: Analyses of elastic scattering cross sections

Lauro Tomio

Instituto de Física Teórica, UNESP
01140-070, São Paulo, SP, Brasil
lauro.tomio@unesp.br

August 09-14, 2026, ECT*, Trento, Italy

ECT* EUROPEAN CENTRE FOR THEORETICAL STUDIES IN NUCLEAR PHYSICS AND RELATED AREAS
FONDAZIONE BRUNO KESSLER

Nuclear Physics under the low-energy, high intensity frontier



Instituto de Física Teórica, Universidade Estadual Paulista (IFT-UNESP),

São Paulo, Brazil

Supported by a thematic project of FAPESP

The main researchers are Arnaldo Gammal, Airton Deppman and myself. It includes topics in Nuclear and Atomic Few-Body Systems, Bose-Einstein Condensation, Nonlinear Dynamics, and Hadronic Physics.

Structural Correction in the Optical Model

Explicitly embedding projectile halo structures via double-folding formalism to resolve the Breakup Threshold Anomaly in weakly bound nuclei.

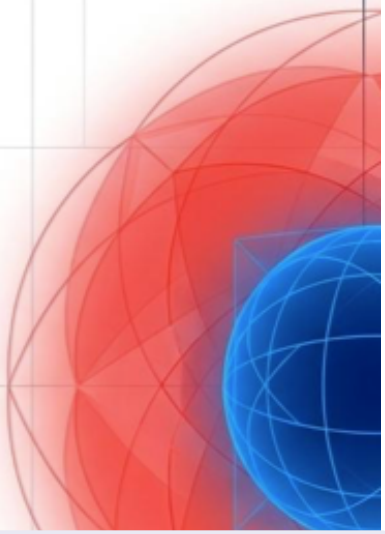

I will report a study in which an explicit treatment of the projectile halo structure within the optical model (OM) provides a more realistic and accurate description of elastic scattering involving weakly bound nuclei.

These underlines that, for a reliable description of elastic-scattering observables and reaction dynamics, one should consider the structural properties of halo projectiles in OM analyses.

Our approach is validated by verifying the Coulomb-nuclear interference peak suppression in halo configurations of ^{8}B and ^{11}Be projectiles in heavy targets.

Main collaborators in the reported work:

- **Bahati Mukeru** (UNISA, Johannesburg, South Africa)
- Joshua T. Majekodunmi (UNISA, Johannesburg, South Africa)
- Valdir Guimarães (Universidade de São Paulo, São Paulo, Brazil)

General remarks on the studies with weakly-bound halo-nuclei projectiles

Astrophysics relevance -

Studies of halo-nuclei reactions with heavy nuclei can be seen as a cornerstone of modern nuclear astrophysics. By revealing the behavior of matter under extreme conditions, they provide fundamental data to answer profound questions about the cosmic origin of the elements and the evolution of stars.

- **Rapid neutron capture processes (r-Processes):**
  R-processes involve rapid succession of neutron captures, creating highly unstable, neutron-rich nuclei far from stability.
- **Impact on predicted final abundance of elements:**
  The unusual structure of halo nuclei can significantly alter their reaction rates. By incorporating into astrophysical models of the r-process, they can change the predicted final abundance of elements.
- **Probing reaction dynamics and rates:**
  - The Coulomb breakup method of a halo nucleus in the intense electric field of a heavy target.
  - Enhancement of Fusion with heavy targets.
  - Whether composed of neutrons or protons, halo effects can lead to different fusion enhancement or suppression effects.

Experimental techniques

The experimental techniques used to study reactions with the weakly-bound projectiles, such as ^{11}Be (neutron halo) and ^{8}B (proton halo), are sophisticated and designed to probe their exotic structures.
The focus approaches are on **breakup reactions**, **elastic scattering**, and, to a lesser extent, **transfer reactions**.
Facilities: ISOLDE at CERN and JYFL (University of Jyväskylä, Finland).

Elastic scattering as a probe of dynamics

Elastic scattering experiments, where the projectile scatters off a target without changing its internal state, are also crucial. They help reveal how the weakly-bound halo structure influences the reaction dynamics.

By measuring the angular distribution of the scattered projectiles and comparing it to theoretical models, they could **isolate the effect of breakup coupling**. The study found that the neutron halo of ^{11}Be produced a much stronger coupling effect than the proton halo of ^{8}B.

These studies relies heavily on breakup reactions to extract structural information, elastic scattering to understand reaction dynamics, and various complementary techniques to fully characterize these exotic systems.

Optical model approaches

The most direct and straightforward interaction between colliding nuclei is given by the elastic scattering, usually analyzed within OM approaches. It provides a fundamental benchmark for understanding more complex reaction channels, as transfer and breakup.

A fundamental OM assumption is that the interaction between structureless colliding nuclei can be described by an average potential representing the nucleon–nucleon interactions within each nucleus, which is modeled by a complex optical potential, whose real part represents the average nuclear interaction, while the imaginary part accounts for the loss of flux from the elastic channel to other reaction channels.

As such, the imaginary part reflects a variety of reaction dynamics and structures, including nuclear structure and channel couplings.

THE STANDARD ASSUMPTION

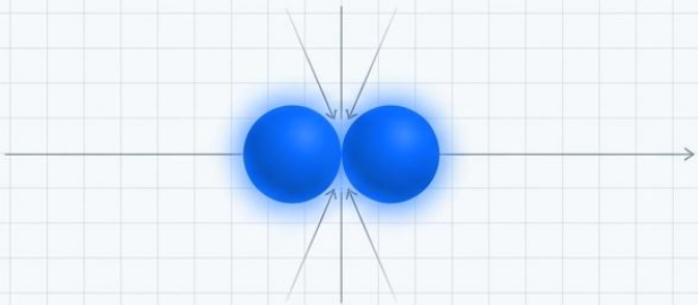

The standard **Optical Model (OM)** treats interacting nuclei as structureless, compact entities.

THE REALITY OF WEAKLY BOUND NUCLEI

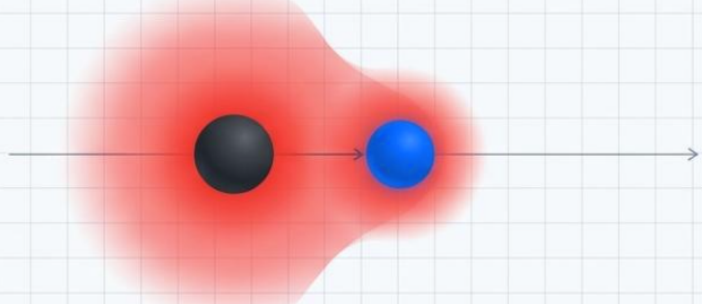

Halo projectiles possess a **diffuse spatial geometry** that fundamentally alters interaction mechanics at vast distances.

THE WOODS-SAXON LIMITATION

Phenomenological form factors (Woods-Saxon) represent average nuclear interactions but are structurally blind. They fail to account for the actual nuclear density distributions of weakly bound partners, forcing artificial renormalizations linked to the **Breakup Threshold Anomaly** (BTA).

Woods-Saxon form factor

The Woods-Saxon (WS) form factor has traditionally been used for both the real and imaginary parts. However, its main limitation is that it does not account for important features of the interacting nuclei, such as nuclear density and other reaction dynamics.

To address the shortcomings of the Woods-Saxon potential, various double-folded (DF) nucleus-nucleus potentials have been developed based on the nuclear densities of the interacting partners, as well as the nucleon-nucleon interaction.

Usually, these potentials are renormalized by the corresponding N_R and N_I (for the real and imaginary parts, respectively) factors to fit the experimental data.
For weakly bound nuclei, the normalization requirement is linked to the breakup threshold anomaly (BTA), which is associated with the energy dependence of the optical potential.

Among these DF potentials, notable examples include the São Paulo potential:
M. A. Cândido Ribeiro, L. C. Chamon, D. Pereira, M. S. Hussein, and D. Galetti, PRL **78**, 3270 (1997).
Based on the M3Y-Paris, M3Y-Reid and M3Y-Fetal, we can mention the following:

- N. Anantaraman, H. Toki, and G. Bertsch, NPA **398**, 269 (1983).
- G. Bertsch, J. Borysowicz, H. McManus, and W. G. Love, NPA **284**, 399 (1977).
- J. O. Fiase, K. R. S. Devan, and A. Hosaka, PRC **66**, 014004 (2002).

For DF density-dependent potentials, from realistic interactions, see:

- G. R. Satchler and W. G. Love, Phys. Rep. **55**, 183 (1979).
- D. T. Kho, G. R. Satchler, W. von Oertzen, PRC **56**, 954 (1997).

The renormalization of the real and imaginary parts of Woods-Saxon potentials

is a standard procedure in nuclear physics, primarily used when comparing a phenomenological Woods-Saxon potential with a more fundamental one, like a microscopic double-folding potential. The core idea is to adjust the strength of the potential's real and imaginary components by multiplying them with normalization factors (often denoted as N_R and N_I or similar) to better fit experimental data, most commonly elastic scattering cross-sections.
In practice, a theoretical or "starting" potential is calculated from first principles using a microscopic model. This initial potential often needs to be scaled for it to accurately reproduce experimental observations.
How the Renormalization Factors are Applied
In an optical model analysis, the complex nuclear potential is typically expressed as: $V_{\text{Nucl}}(r) = V_R(r) - iW_I(r)$, where V_R is the real part (average nuclear potential) and W_I is the imaginary part (absorption into reaction channels).
When comparing a Woods-Saxon potential to a potential from a folding model, the procedure is to multiply the real and i maginary parts of the microscopic potential by separate renormalization factors, to fit the elastic scattering data, as

$$N_R\, V_{\text{Folding}} - i\, N_I\, W_{\text{Folding}}\,.$$

Empirical Findings on Renormalization Values
The N_R and N_I are not fixed; they depend on the specific reaction, energy, the nuclei involved, and the particular microscopic model.
An analysis of $^{12,13}\mathrm{C}$ scattering on $^{90,91,92,94,96}\mathrm{Zr}$ at 64 MeV found that the renormalization needed vary:

- For the SPP2 (São Paulo Potential version 2) and BNP (Brazilian Nuclear Potential), the real part required little to no renormalization ($N_R = 1$), while the imaginary part needed to be reduced to about 78–90% ($N_I = 0.78$ to 0.9).
- For the CDM3Y6 (Complex Density-dependent Michigan-3-Yukawa) potential, more significant reductions were needed for both parts: $N_R = 0.6$ to 0.8 and $N_I = 0.4$ to 0.8 for $^{12}\mathrm{C}$, and $N_R = 0.7$ to 1 and $N_I = 0.4$ to 0.8 for $^{13}\mathrm{C}$.

In **summary**, the renormalization of the real and imaginary parts of Woods-Saxon potentials is a practical tool used to bridge the gap between sophisticated theoretical models and experimental reality. The specific values of the renormalization factors are extracted by fitting data and provide insight into the adequacy of the underlying microscopic model, with values significantly different from 1 suggesting the model may be missing important physics.

The status on the structure and reactions of neutron-rich nuclei was reviewed in C. A. Bertulani, L. F. Canto, M. S. Husssein, in Phys. Rep. **226**, 281 (1993). Particularly, they have considered the properties of ^{11}Li.

Also, a lower-order correction of the density dependence of in-medium nucleon-nucleon cross sections, obtained from geometrical considerations of Pauli-blocking effects, is proposed by Bertulani in J. Phys. G **27** L67 (2003).

Nucleus-nucleus double-folded potential

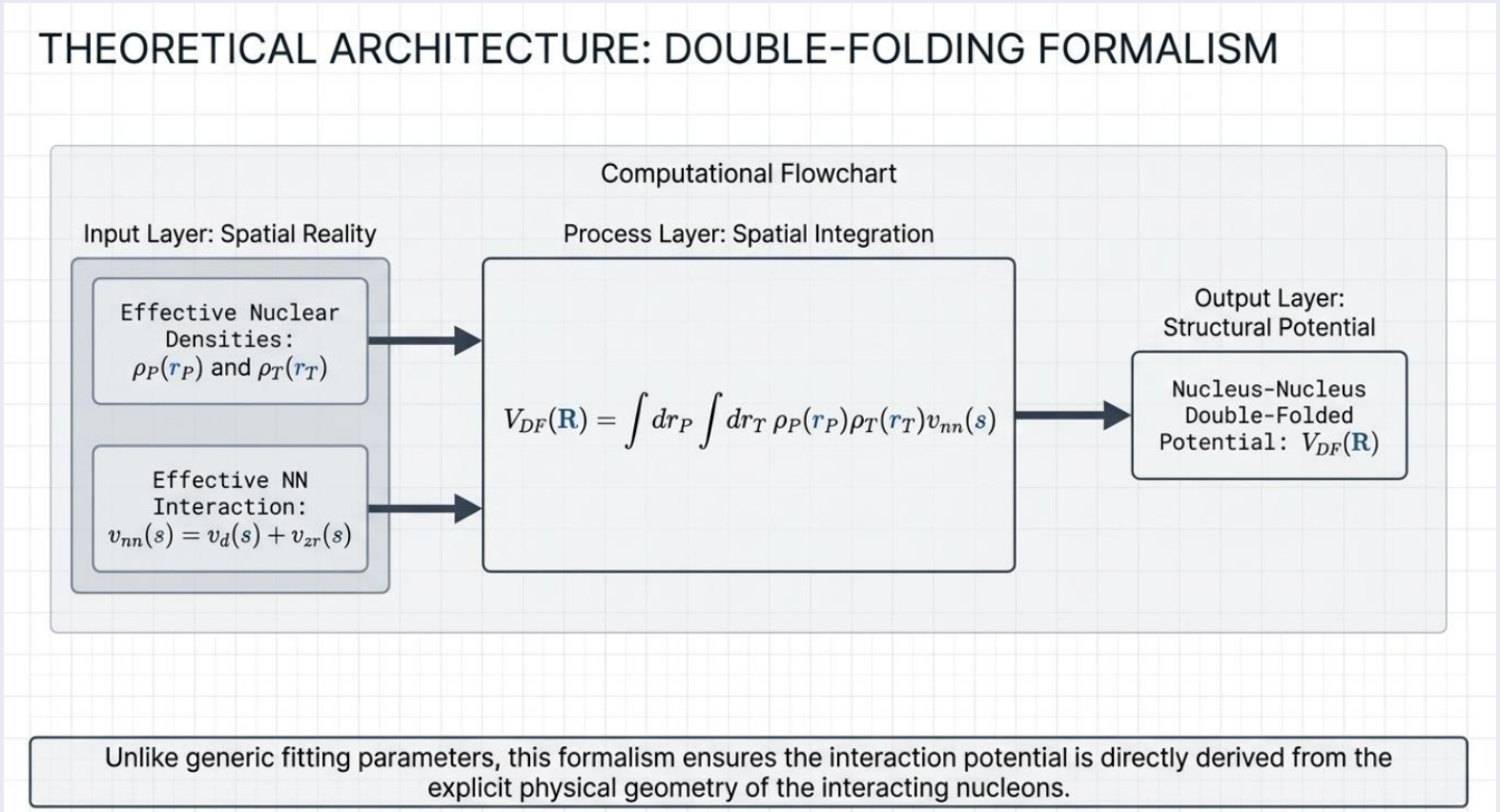

where **R** gives the separation vector between the centers of mass of the projectile and target nuclei, with $\mathbf{r_P}$ and $\mathbf{r_T}$ being the internal coordinates of nucleons - projectile and target - relative to their center of mass.

With $\mathbf{s} \equiv \mathbf{R} - \mathbf{r_T} + \mathbf{r_P}$, such that the relative distance between a nucleon of the projectile from a nucleon in the target is $s = |\mathbf{s}|$, the nucleon-nucleon (nn) effective interaction $v_{nn}(\mathbf{s})$ is defined by the sum of a direct term $v_d(s)$ and an exchange one $v_{zr}(\mathbf{s})$, which is assumed having zero-range:

$$v_{nn}(\mathbf{s}) \quad = \quad v_d(s) + v_{zr}(\mathbf{s}) = \left[V_r \frac{e^{-\mu_r s}}{\mu_r s} - V_a \frac{e^{-\mu_a s}}{\mu_a s} \right] + J_{00}(E)\delta^3(\mathbf{s}),$$

where $J_{00}(E) \equiv \kappa \left(1 - \gamma_0 \frac{E}{A_P}\right)$, with V_r, V_a, μ_r and μ_a given by different nn models. E is the incident energy, A_P the projectile mass number, with the parameters κ and γ_0 given in the next Table.

Numerical values of the parameters of the different *nn* interactions

The *nn* parametrizations are given in Ochala and Fiase, PRC **98**, 064001 (2018), with M3Y-Reid in Bertsch, et al. NPA **284**, 399 (1977), Kobos, et al., NPA **384**, 65 (1982), M3Y-Paris in Anantaraman, et al., NPA **398**, 269 (1983), and B3Y-Fetal in Fiase, et a., PRC **66**, 014004 (2002).

Interaction	V_r (MeV)	μ_r (fm^{-1})	V_a (MeV)	μ_a (fm^{-1})	κ ($MeV.fm^3$)	γ_0 (MeV^{-1})
M3Y-Reid	7999	4	2134	2.5	-276	0.005
M3Y-Paris	11062	4	2538	2.5	-590	0.002
B3Y-Fetal	10472	4	2203.11	2.5	-590	0.002

DF potential

Considering the Fourier transforms of the effective nuclear densities and the *nn* interaction, the double-folded potential can be transformed as

$$V_{DF}(R) = \frac{1}{2\pi^2 R} \int F_P(q) F_T(q) F_{nn}(q) \sin(qR) q dq,$$

where $F_P(q)$, $F_T(q)$ and $F_{nn}(q)$ are the respective projectile, target and nn interaction Fourier transforms:

$$\begin{pmatrix} F_P(q) \\ F_T(q) \\ F_{nn}(q) \end{pmatrix} = \frac{4\pi}{q} \int \begin{pmatrix} \rho_P(r) \\ \rho_T(r) \\ v_{nn}(r) \end{pmatrix} \sin(qr) r dr.$$

Assuming a compactless core, centered at the cm with negligible core recoil, the density of the projectile halo nucleus can be obtained from 2 terms:

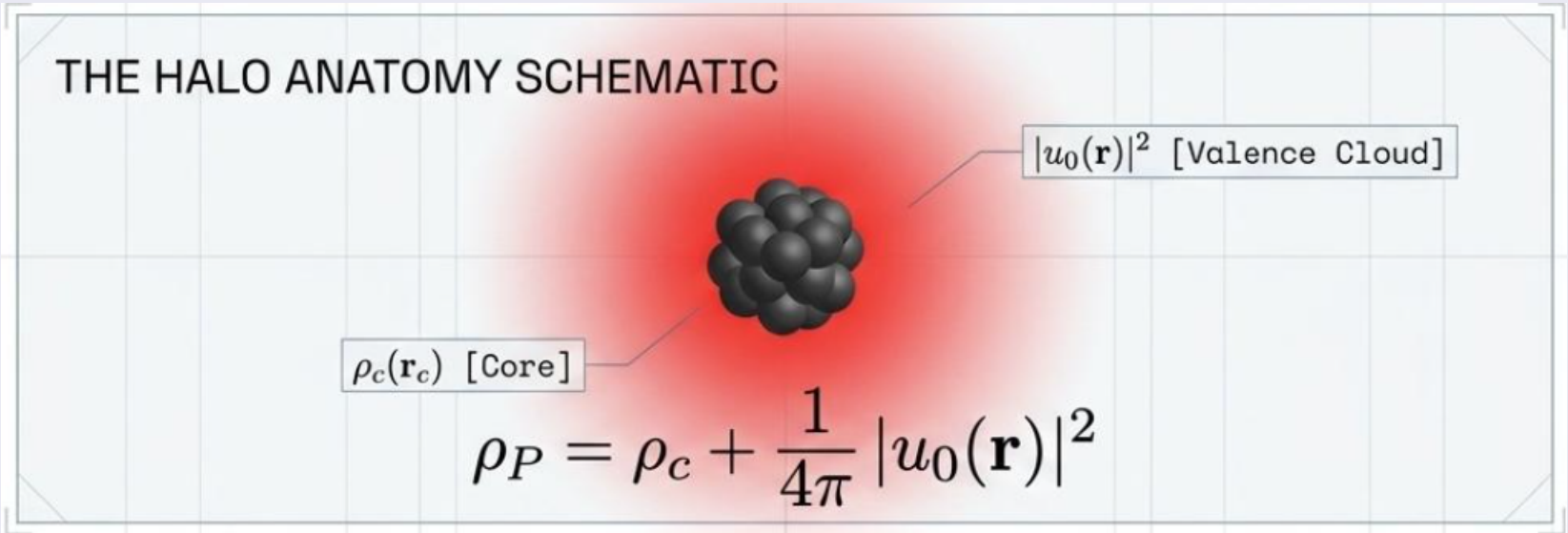

where $u_0(r)$ the ground-state wave function of the core-nucleon system. So, the density $\rho_P(\mathbf{r_p})$ contains the halo structure through $u_0(r)$.

With ρ being the overlapping density in the nuclear medium of both nuclei, the effective density-dependent nn interaction is

$$v_{nn}(\rho, E, \mathbf{s}) \quad = \quad [v_d(s) + v_{zr}(s)]\, C[1 + \alpha e^{-\beta\rho} - \gamma\rho].$$

The parameters C, α, β, γ are fitted to ensure the saturation of nuclear matter, and to reproduce the correct values of the nuclear matter binding $B_0 \approx 16$ MeV at $\rho_0 \approx 0.17$ fm^{-1}.

Parameters of the function for different M3Y-Paris interactions:

Interaction	C	α	$\beta(\mathrm{fm}^3)$	$\gamma(\mathrm{fm}^3)$.
BDM3Y1	1.2521	0.0	0.0	1.7452
CDM3Y4	0.3052	3.2998	2.3180	2.0
DDM3Y1	0.2963	3.7231	3.7384	0.0

The Fourier transform of the direct and zero-range terms with the density-dependent *nn* interaction

$$
\begin{aligned}
V_{DF}^{Dd}(R) &= \frac{C}{2\pi^2 R}\int \Big[F_P(q)F_T(q) + \alpha F_P(q)F_T(q) \\
&\qquad -\gamma G(q)\Big] F_{nn}(q)\sin(qR)qdq, \\
V_{DF}^{Dzr}(R) &= \frac{CJ_{00}(E)}{2\pi^2 R}\int \Big[F_P(q)F_T(q) + \alpha F_P(q)F_T(q) \\
&\qquad -\gamma G(q)\Big] \sin(qR)qdq,
\end{aligned}
$$

where $F_P(q)$, $F_T(q)$ are the density functionals. The $G(q)$ is given by

$$
G(q) = \frac{4\pi}{q}\int [\rho_P(r) + \rho_T(r)]\sin(qr)rdr.
$$

Optical potential

The optical potential can be written by a Coulomb-nuclear sum:

$$\begin{aligned} U_{pt}(R) &= V_C(R) + U_N(R) \\ &= V_C(R) + N_R V_{DF}(R) + \mathrm{i} N_I W_{DF}(R), \end{aligned}$$

where $V_C(R)$ is the Coulomb component, with the nuclear component , N_R and N_I are normalization coefficients, which will be obtained through a fitting of the elastic scattering to experimental data.

The normalization factors N_R and N_I are meant to simulate a range of reaction dynamics.

Our approach

For the weakly-bound halo nuclei, for comparison, we have assumed the ^{11}Be (Beryllium-11) and ^{8}B (Boron-8).

^{8}B is a radioactive isotope of boron that features a proton halo, where a valence proton orbits a core of ^{7}Be ($^{8}\mathrm{B} = {}^{7}\mathrm{Be}{+}p$).

^{11}Be is a radioactive isotope of beryllium, with 4 protons and 7 neutrons, As a one-neutron halo nucleus it can be assumed with a ^{10}Be core, with a neutron halo: ($^{11}\mathrm{Be} = {}^{10}\mathrm{Be}{+}n$).

The ^{7}Be and ^{10}Be densities were computed using the Dirac-Hartree-Bogoliubov (DHB) model [See, B. V. Carlson, D. Hirata, Phys. Rev. C **62**, 054310 (2000), Chamon, Carlson, Gasques, CPC 267 (2021) 108061].
For the non-halo configuration, the densities of $^{11}\mathrm{Be}$ and $^{8}\mathrm{B}$ were obtained from the same DHB approach; particularly well suited for weakly bound nuclei, as also includes pairing correlations.

Recent elastic scattering calculations [Hatano et al. J. Phys. G **52**, 075102 (2025)], demonstrated that realistic DHB densities yields improved results over phenomenological density parametrizations.

A systematic comparison among different density prescriptions would be valuable to further clarify this aspect.

As we are only considering the effect of the ground-state on the elastic scattering, the $p_{1/2^-}$ excited state of the ^{11}Be was excluded.

The rms radii ($\sqrt{\langle r^2 \rangle}$) (in fm) for the ^{8}B and ^{11}Be nuclei

The rms together with the respective matter radii of their core nuclei, within the halo and non-halo configurations. The available experimental values, provided in the third row.

	$^{8}\mathrm{B}_{\mathrm{halo}}$	$^{8}\mathrm{B}$	$^{11}\mathrm{Be}_{\mathrm{halo}}$	$^{11}\mathrm{Be}$	$^{7}\mathrm{Be}$	$^{10}\mathrm{Be}$
$\langle r^2 \rangle^{\frac{1}{2}}$	2.65	2.60	3.18	2.63	2.34	2.49
Exp	2.58±0.06	–	2.90±0.05	–	2.31±0.05	2.28±0.02

Nuclear densities

Nuclear densities for ^{11}Be within halo (red-solid lines) and non-halo configurations (blue-dot-dashed lines). The corresponding core-nuclei and valence nucleon densities are also provided.

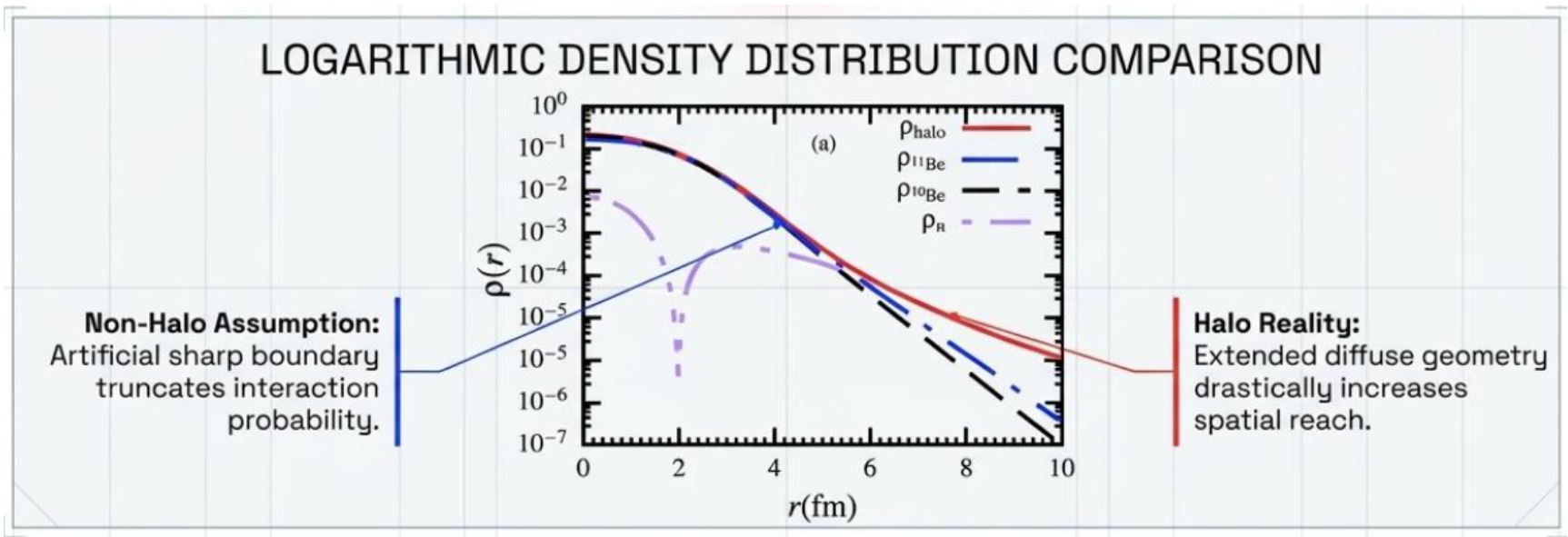

Nuclear densities

Nuclear densities for both ^{8}B within halo (red-solid lines) and non-halo configurations (blue-dot-dashed lines). The corresponding core-nuclei and valence nucleon densities are also provided.

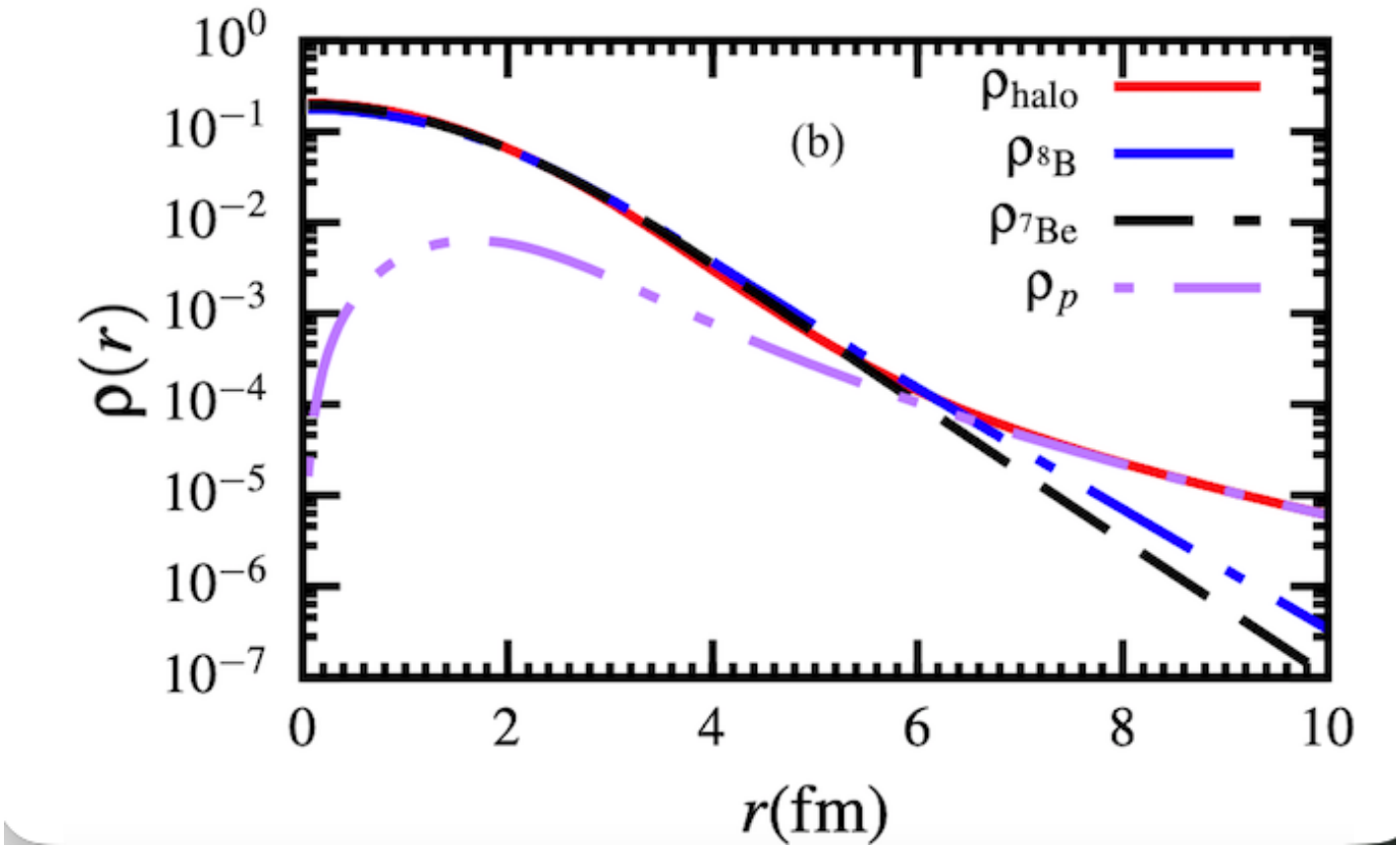

Coulomb barrier heights

Coulomb barrier heights for the ^{8}B and ^{11}Be on the target nuclei ^{64}Zn and ^{208}Pb. Assuming halo ($V_{^{8}\mathrm{B}_{\mathrm{halo}}}$ and $V_{^{11}\mathrm{Be}_{\mathrm{halo}}}$) and non-halo ($V_{^{8}\mathrm{B}}$ and $V_{^{11}\mathrm{Be}}$) configurations for different *nn* interactions (v_{nn}).

	v_{nn}	$V_{^{8}\mathrm{B}_{\mathrm{halo}}}$	$V_{^{8}\mathrm{B}}$	$V_{^{11}\mathrm{Be}_{\mathrm{halo}}}$	$V_{^{11}\mathrm{Be}}$
^{64}Zn	M3Y-Paris	20.02	20.51	14.66	15.69
	M3Y-Reid	20.22	20.70	14.85	15.82
	B3Y-Fetal	20.67	21.12	15.28	16.08
	DDM3Y1	20.05	20.48	14.87	15.75
	BDM3Y1	19.83	20.31	14.81	16.18
	CDM3Y4	20.01	20.46	14.86	15.77
^{208}Pb	M3Y-Paris	47.05	47.97	35.05	36.92
	M3Y-Reid	47.47	48.36	35.44	37.18
	B3Y-Fetal	48.38	49.21	36.30	37.71
	DDM3Y1	47.28	48.09	35.52	37.10
	BDM3Y1	46.66	47.55	35.31	37.89
	CDM3Y4	47.13	47.97	35.44	37.11

Geometry Dictates Potential

The ground-state wave function of the core-nucleon system natively stretches the interaction range. By feeding the extended density tail into the double-folding integral, the resulting nuclear force naturally reaches further outward.

Halo Configuration

Non-Halo Configuration

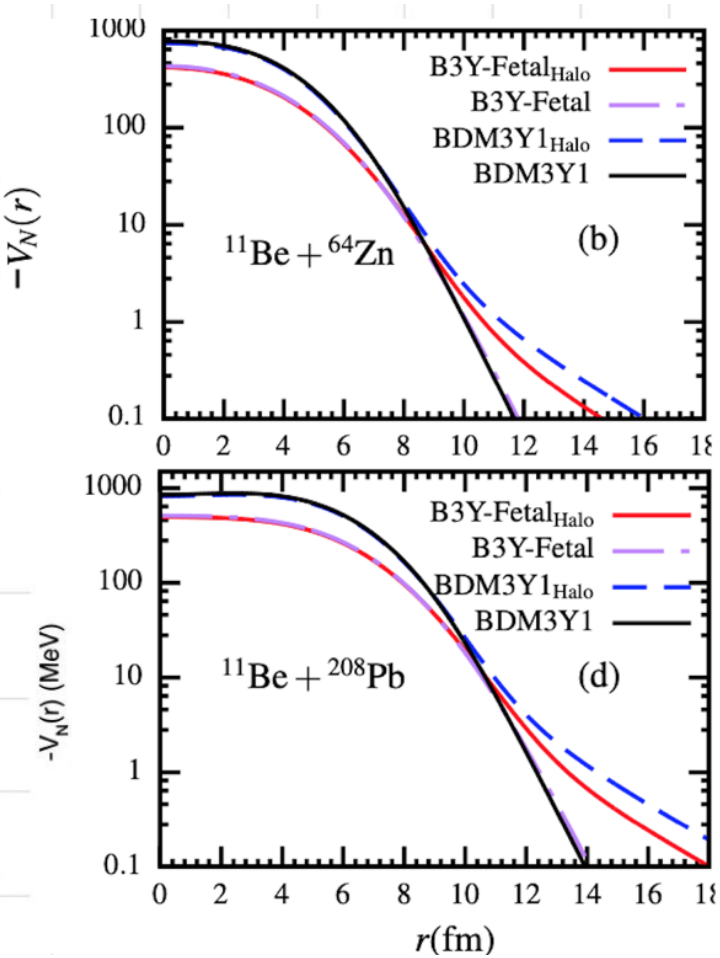

Nuclear potentials

Nuclear potentials for the $^{11}\mathrm{Be} + {}^{64}\mathrm{Zn}$ [(a), (b)] and $^{11}\mathrm{Be} + {}^{208}\mathrm{Pb}$ [(c), (d)], with ^{11}Be treated as a halo nucleus, using various nn interactions. (b) and (d) show the potentials from (a) and (c) on a log scale.

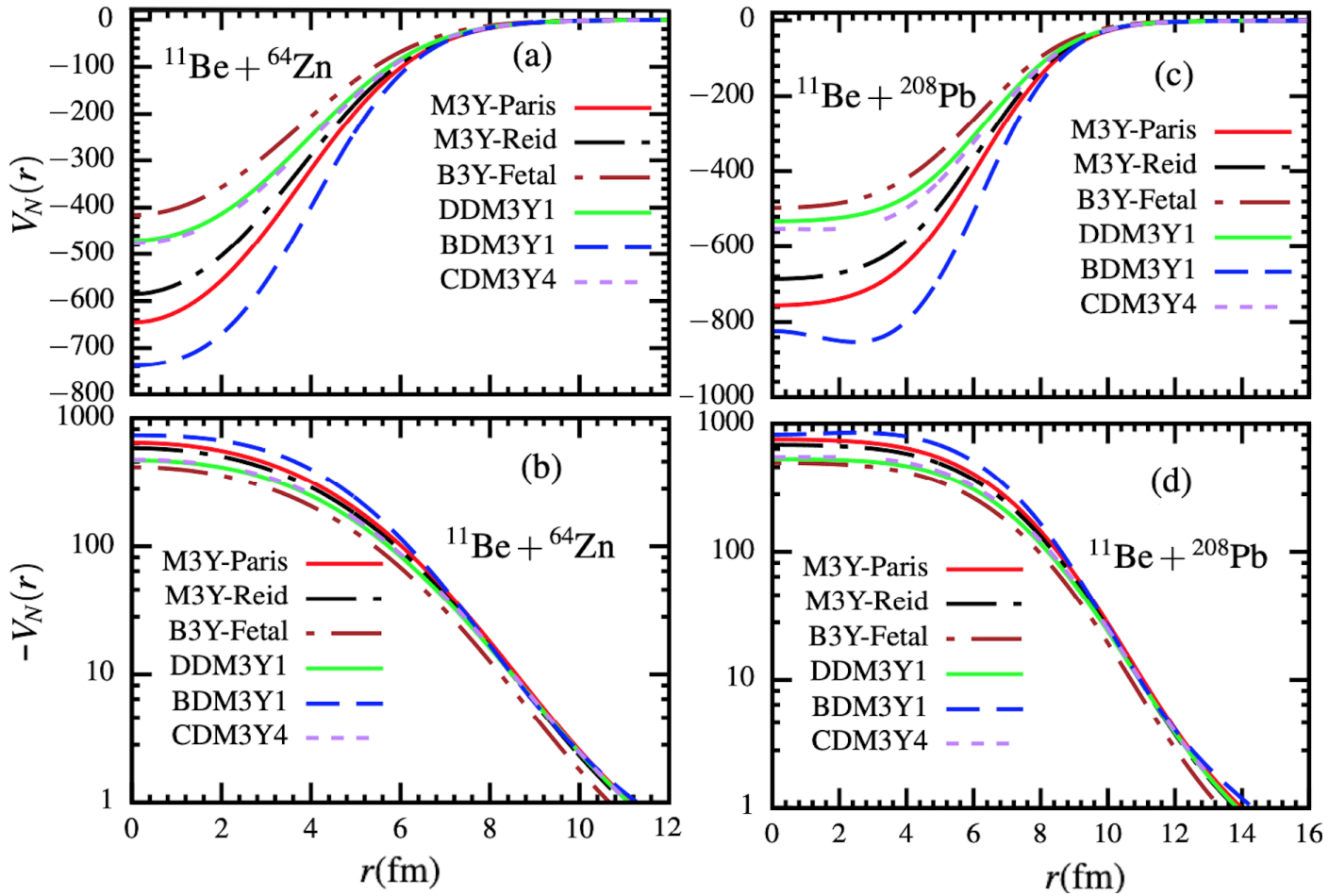

Nuclear potentials for the $^{11}\mathrm{Be} + {}^{64}\mathrm{Zn}$ [(a), (b)] and $^{11}\mathrm{Be} + {}^{208}\mathrm{Pb}$ [(c), (d)], by treating ^{11}Be in the halo and non-halo configurations and using the B3Y-Fetal and BDM3Y1 nn interactions. (b) and (d) are in log scales.

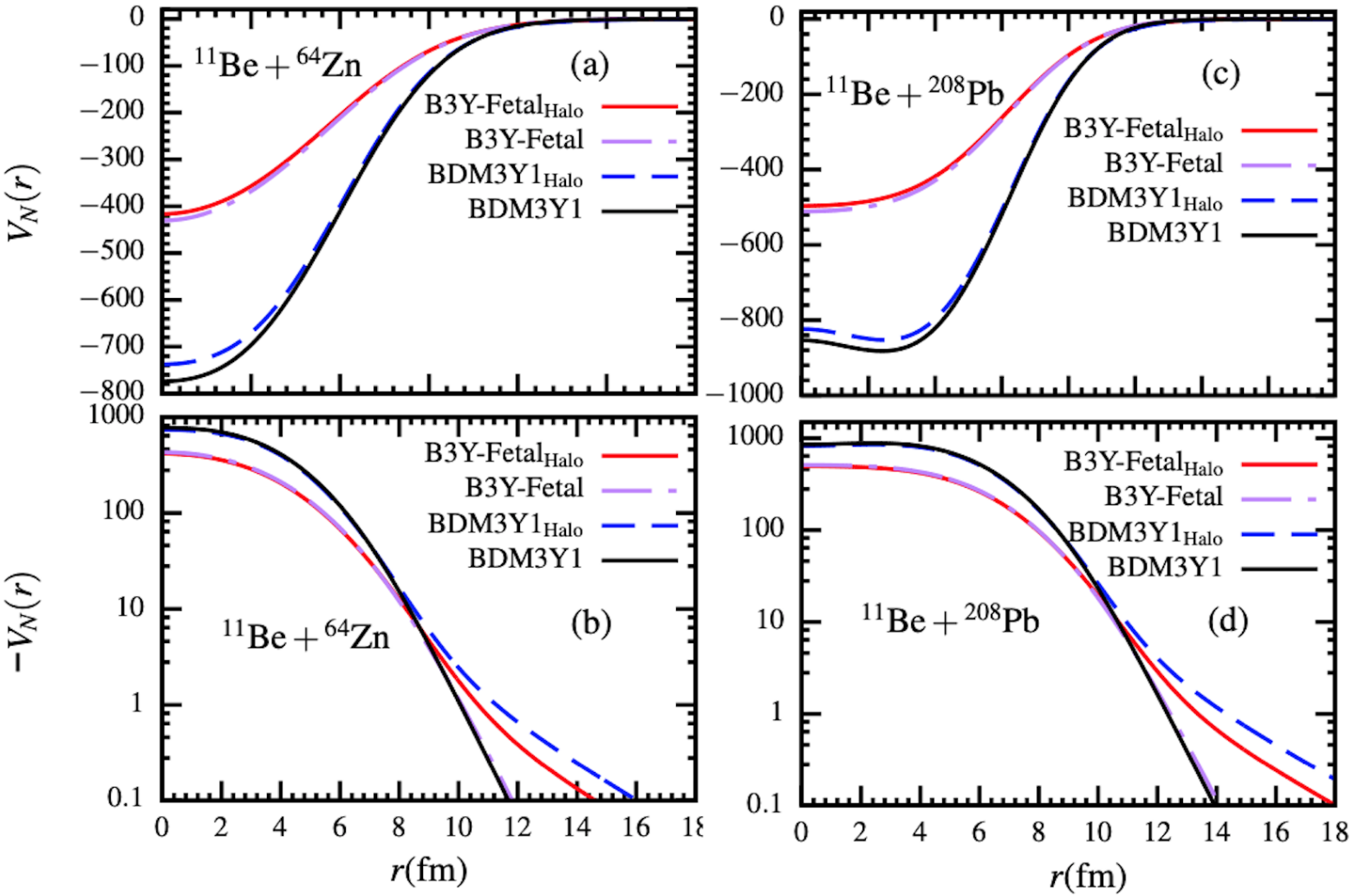

	Phenomenological (Woods-Saxon)	Double-Folded Halo Formalism
Structure Phase	Structureless. Assumes perfectly compact, opaque interacting spheres.	Structure-aware. Explicitly models core + valence nucleon probability distributions.
Potential Derivation	Generic mathematical form factors adjusted purely by retrospective data fitting.	$U_{pt}(R) = V_C(R) + N_R V_{DF}(R) + N_I V_{DF}(R)$
Normalization Integrity	Highly volatile. Highly susceptible to artificial parameter inflation to mask Breakup Threshold Anomalies.	Tightly constrained. Anchored to actual nuclear matter densities and nucleon-nucleon phase space.

Empirical Validation: Halo Suppression of Interference

Non-Halo Configuration (^{11}Be + ^{64}Zn)

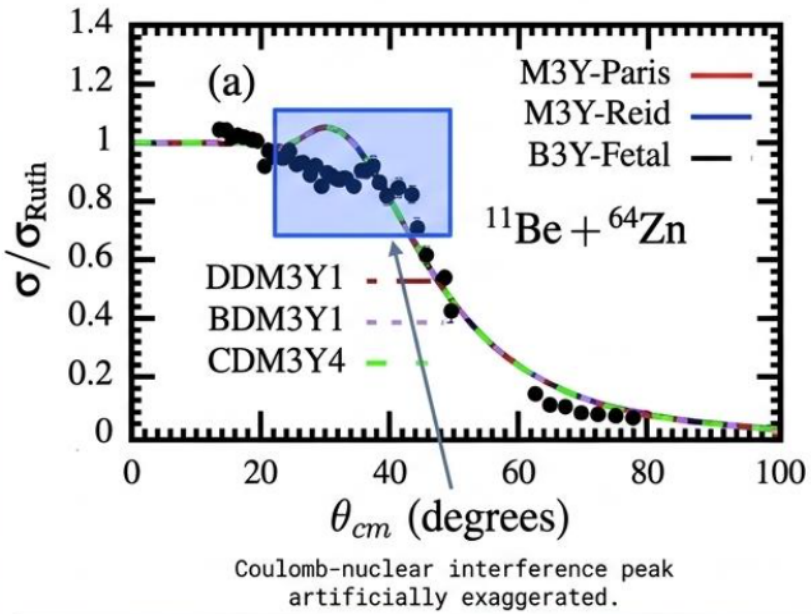

Coulomb-nuclear interference peak artificially exaggerated.

Halo Configuration (^{11}Be + ^{208}Pb)

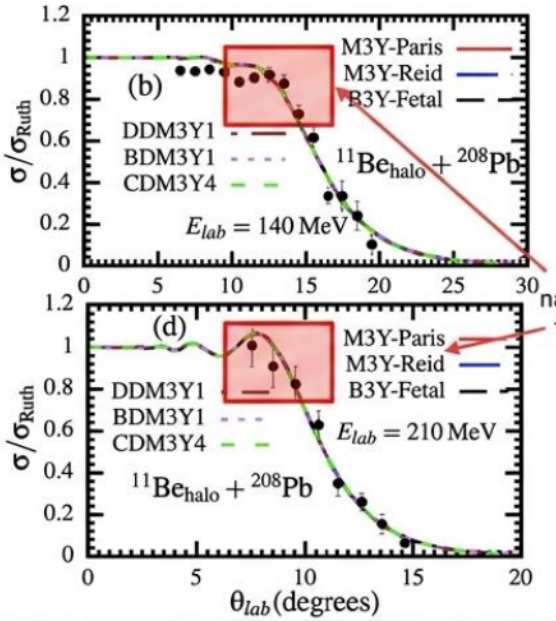

Halo configuration naturally suppress the interference peak.

Empirical Validation: Introducing the extended tail of the halo wave function naturally suppresses the Coulomb-nuclear interference peak, bringing models into perfect alignment with experimental cross-sections without forced parameter distortion.

Elastic scattering cross-sections σ (units of σ_{Ruth})

$\sigma/\sigma_{\rm Ruth}$, for $^{11}\mathrm{Be} + {}^{64}\mathrm{Zn}$, at incident $E_{cm} = 24.5$ MeV, with different *nn* interactions. (a) shows the ^{11}Be as a non-halo, while (b) corresponds to the halo configuration. Data from Di Pietro *et al.*, PRL **105**, 022701 (2010).

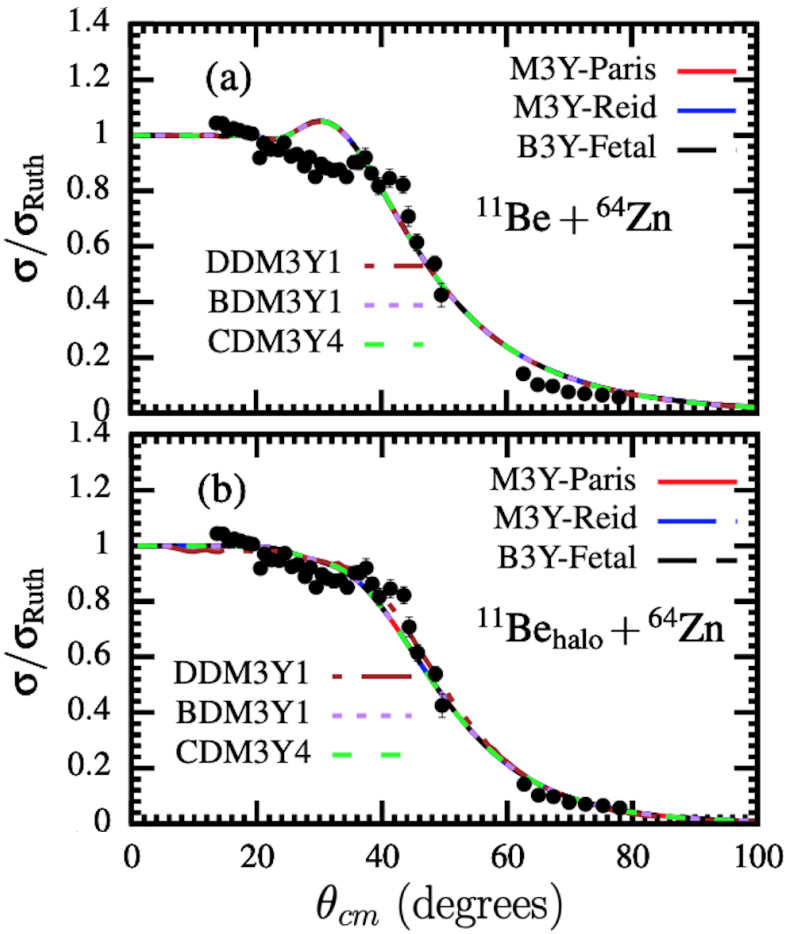

$\sigma/\sigma_{\rm Ruth}$, for $^{11}\mathrm{Be} + {}^{208}\mathrm{Pb}$, at E_{lab} =140 MeV [(a) and (b)] and 210 MeV [(c) and (d)], with different *nn* interactions. (a) and (c) correspond to the non-halo, while (b) and (d) correspond to the halo configuration for ^{11}Be. Data from F. F. Duan *et at* ., PLB **811**, 135942 (2020); PRC **105**, 034602 (2022).

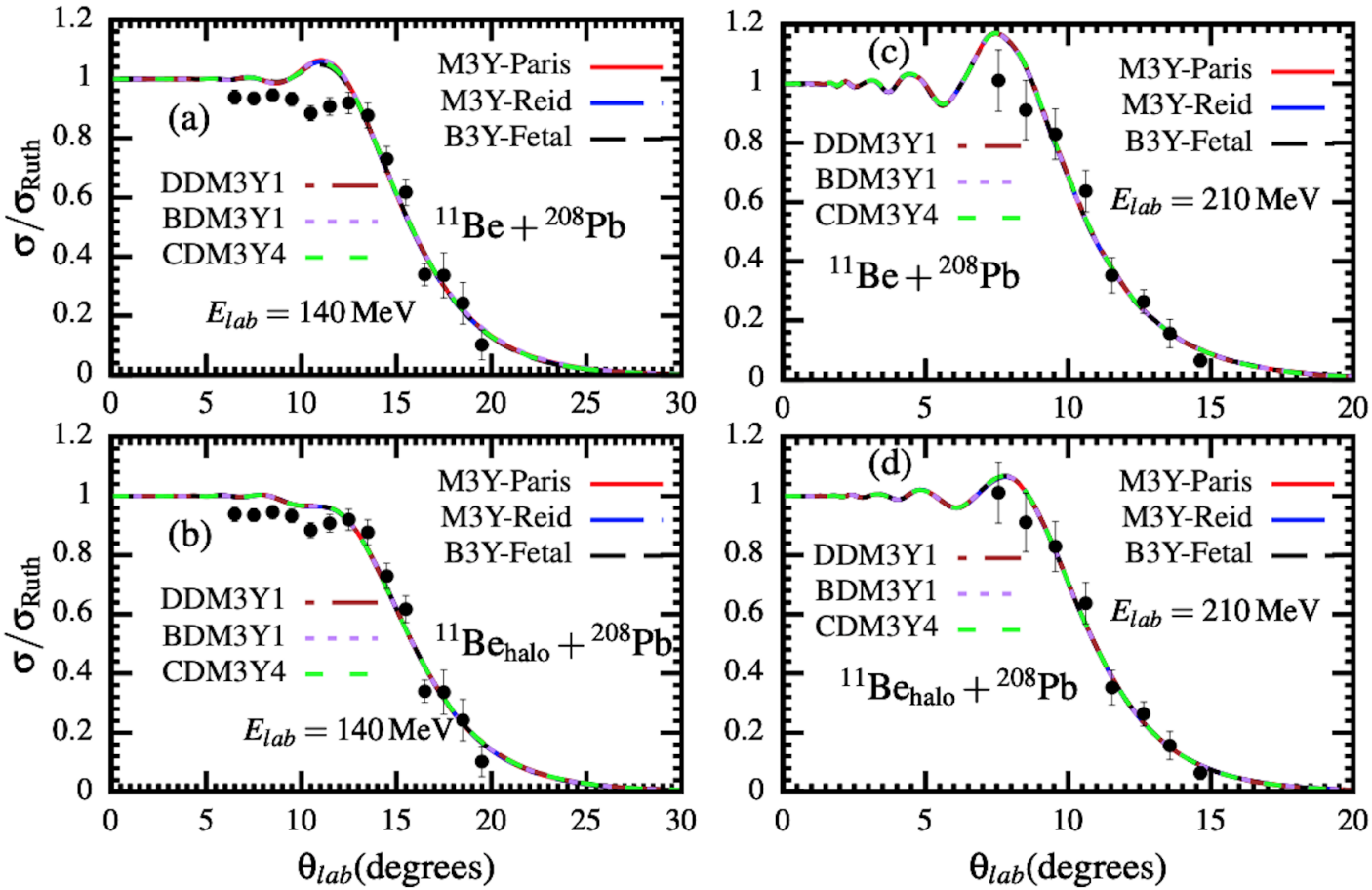

$\sigma/\sigma_{\rm Ruth}$, for the $^{8}\mathrm{B} + {}^{64}\mathrm{Zn}$ at $E_{lab} = 38.5$ MeV, with different *nn* interactions. (a) for ^{8}B treated as a non-halo, while (b) corresponds to the halo configuration. Data from R. Spartà *et al.*, PLB **820**, 136477 (2021).

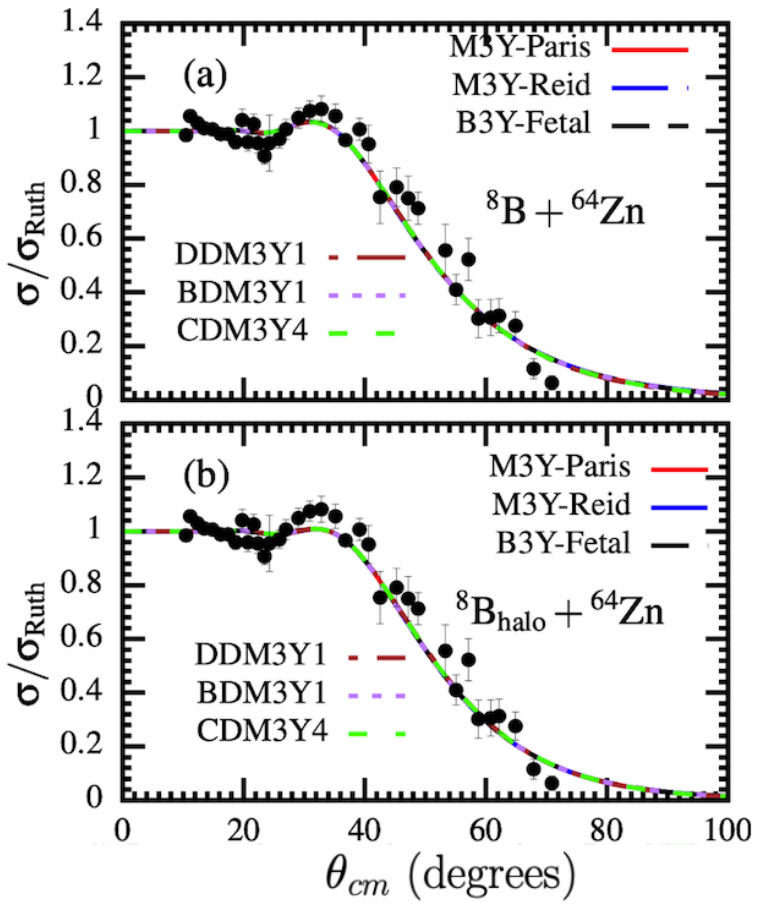

$\sigma/\sigma_{\mathrm{Ruth}}$, for $^{8}\mathrm{B} + ^{120}\mathrm{Sn}$ (Boron projectile + Tin target), at $E_{lab} = 46.1$ and 38.7 MeV, using different *nn* interactions. (a) and (c) correspond to the non-halo, while (b) and (d) correspond to the halo configuration for ^{8}B. Data from L. Yang *et al.*, Nat. Commun. **13**, 7193 (2022).

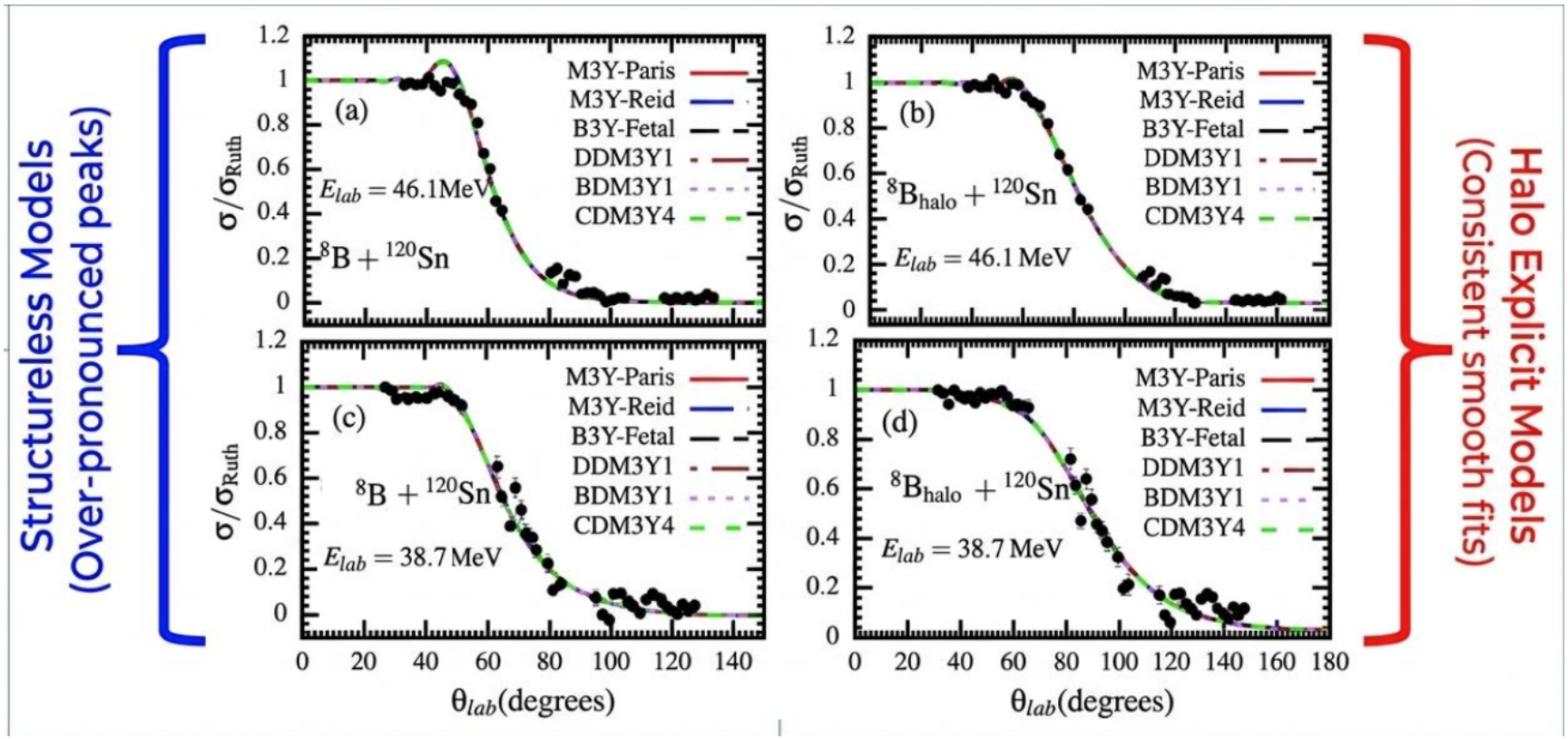

$\sigma/\sigma_{\rm Ruth}$, for $^{8}\mathrm{B} + ^{208}\mathrm{Pb}$ collisions at $E_{lab} = 170.3$ MeV and 238 MeV, with different *nn* potentials. (a) and (c) are for the non-halo, while (b) and (d) correspond to halo configuration for ^{8}B. Data from Wang *et al.*, PRC **103**, 024606 (2021); Yang *et al.*, PRC **87**, 044613 (2013).

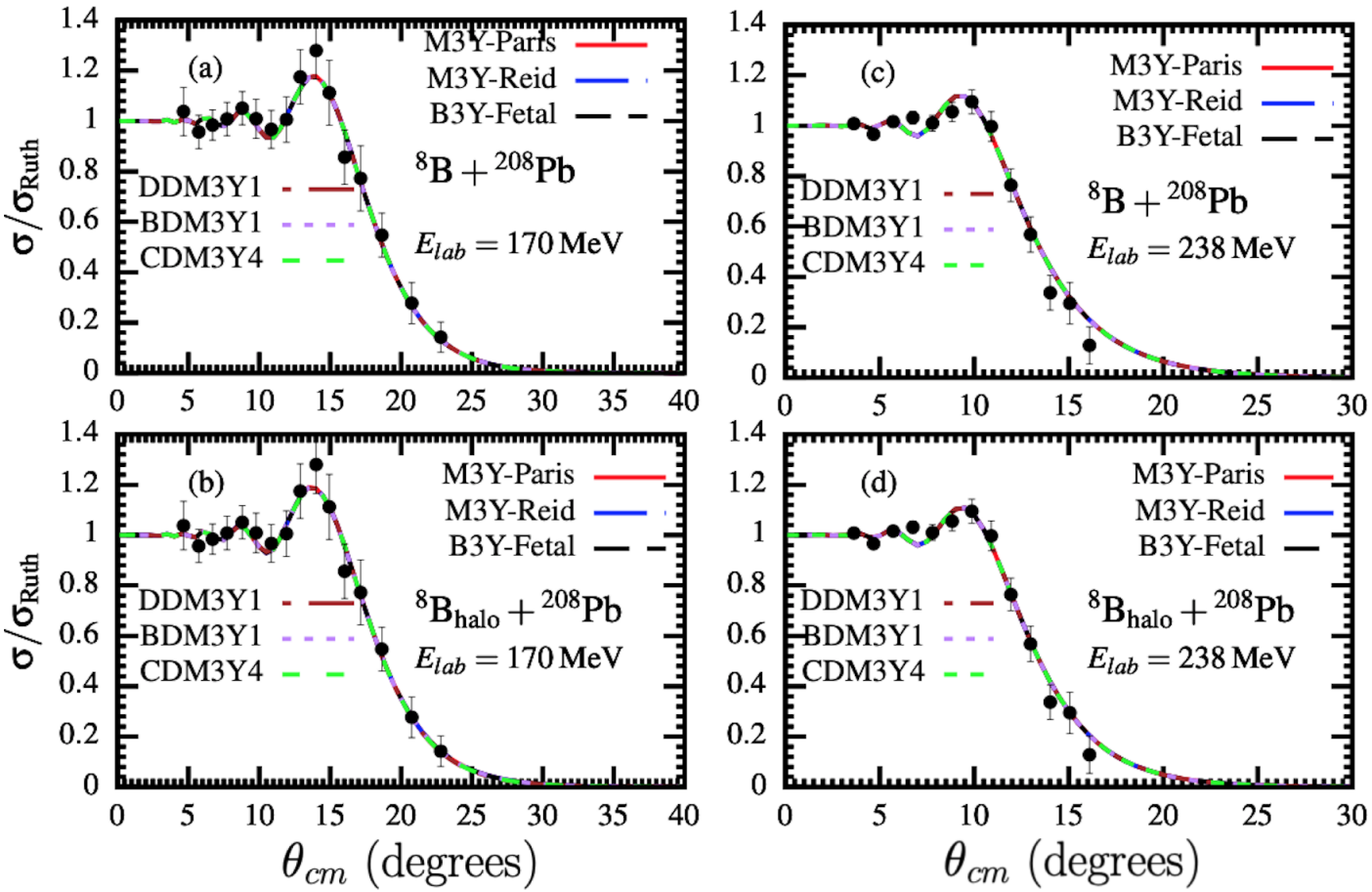

To quantify the static breakup effect on the elastic-scattering dynamics, we performed OM calculations, with the halo and non-halo configurations. N_R and N_I are adjusted to the best fit to experimental data by minimizing χ^2:

$$\chi^2 = \frac{1}{N}\sum_{i=1}^{N}\left[\frac{\sigma_{\rm exp}(E_i) - \sigma_{\rm th}(E_i)}{\sigma_{\rm th}(E_i)}\right]^2.$$

The total cross sections σ_R, considered for each *nn* interaction, are summarized in the following tables for ^{11}Be and and ^{8}B projectiles on each target nucleus.

Fitting N_R, N_I, χ^2, and total reaction cross-sections for the ^{11}Be collision on ^{64}Zn and ^{208}Pb targets for six different nn interactions, within the halo (+) and non-halo (−) configurations of the ^{11}Be.

		Halo configuration				Non-halo configuration			
Reaction	v_{nn}	N_{R+}	N_{I+}	χ^2_+	σ_{R+}	N_{R-}	N_{I-}	χ^2_-	σ_{R-}
$^{11}\mathrm{Be} + {}^{64}\mathrm{Zn}$ $E_{cm} = 24.5$	M3Y-Paris	0.143	0.405	12.649	2232	0.129	3.193	28.001	1795
	M3Y-Reid	0.158	0.447	12.651	2233	0.148	3.534	28.130	1795
	B3Y-Fetal	0.192	0.583	12.721	2232	0.177	4.209	28.021	1796
	DDM3Y1	0.140	0.449	13.065	2193	0.150	3.171	27.977	1795
	BDM3Y1	0.174	0.357	12.869	2192	0.108	5.222	28.845	1789
	CDM3Y4	0.142	0.441	13.038	2193	0.145	3.282	28.089	1794
$^{11}\mathrm{Be} + {}^{208}\mathrm{Pb}$ $E_{lab} = 140$	M3Y-Paris	0.071	0.735	3.445	5498	0.530	1.210	7.278	5033
	M3Y-Reid	0.078	0.818	3.448	5496	0.489	1.168	7.575	5011
	B3Y-Fetal	0.076	1.072	3.480	5485	0.600	1.245	7.048	5038
	DDM3Y1	0.062	0.660	3.815	5411	0.551	1.198	7.390	5011
	BDM3Y1	0.156	0.496	3.683	5417	0.503	1.137	7.894	5032
	CDM3Y4	0.069	0.636	3.795	5412	0.558	1.200	7.364	5011
$^{11}\mathrm{Be} + {}^{208}\mathrm{Pb}$ $E_{lab} = 210$	M3Y-Paris	0.201	0.396	0.570	4716	0.769	1.658	1.284	4277
	M3Y-Reid	0.223	0.443	0.572	4716	0.856	1.845	1.287	4278
	B3Y-Fetal	0.286	0.572	0.579	4706	1.018	2.200	1.271	4274
	DDM3Y1	0.226	0.450	0.537	4690	0.702	1.540	1.220	4269
	BDM3Y1	0.206	0.370	0.499	4741	0.671	1.448	1.274	4270
	CDM3Y4	0.221	0.436	0.539	4694	0.707	1.540	1.245	4270

... within the halo (+) and non-halo (−) configurations of the ^{8}B nucleus.

		Halo configuration				Non-halo configuration			
Reaction	v_{nn}	N_{R+}	N_{I+}	χ^2_+	σ_{R+}	N_{R-}	N_{I-}	χ^2_-	σ_{R-}
$^{8}\mathrm{B} + ^{64}\mathrm{Zn}$ $E_{lab} = 38.5$	M3Y-Paris	0.147	0.577	131	1439	0.039	0.940	132	1352
	M3Y-Reid	0.155	0.639	131	1437	0.044	1.044	132	1352
	B3Y-Fetal	0.186	0.808	131	1429	0.052	1.267	132	1352
	DDM3Y1	0.114	0.684	131	1429	0.039	1.054	132	1350
	BDM3Y1	0.149	0.697	131	1424	0.051	1.063	132	1352
	CDM3Y4	0.109	0.680	131	1425	0.042	1.078	132	1349
$^{8}\mathrm{B} + ^{120}\mathrm{Sn}$ $E_{lab} = 38.7$	M3Y-Paris	0.353	0.820	7.968	1053	0.526	2.584	8.796	939
	M3Y-Reid	0.391	0.907	7.964	1053	0.564	2.836	8.975	939
	B3Y-Fetal	0.453	1.167	7.896	1051	0.691	3.412	8.798	939
	DDM3Y1	0.231	1.088	7.803	1035	0.477	3.003	8.833	938
	BDM3Y1	0.471	0.952	8.398	1037	0.598	4.729	8.920	931
	CDM3Y4	0.247	1.067	7.829	1035	0.477	3.083	8.840	937
$^{8}\mathrm{B} + ^{120}\mathrm{Sn}$ $E_{lab} = 46.1$	M3Y-Paris	0.893	0.708	6.580	1555	1.071	1.388	11.537	1407
	M3Y-Reid	0.990	0.785	6.597	1555	1.185	1.534	11.569	1407
	B3Y-Fetal	1.218	0.998	6.594	1550	1.420	1.860	11.357	1407
	DDM3Y1	0.780	0.894	6.804	1530	0.956	1.610	11.572	1406
	BDM3Y1	0.987	0.853	6.995	1554	1.594	2.382	13.735	1401
	CDM3Y4	0.787	0.881	6.888	1531	0.988	1.637	11.864	1405
$^{8}\mathrm{B} + ^{208}\mathrm{Pb}$ $E_{lab} = 170.3$	M3Y-Paris	0.562	0.492	0.203	3336	0.582	0.680	0.189	3246
	M3Y-Reid	0.621	0.545	0.203	3336	0.643	0.751	0.189	3246
	B3Y-Fetal	0.768	0.686	0.202	3328	0.787	0.919	0.189	3249
	DDM3Y1	0.591	0.541	0.202	3335	0.581	0.682	0.189	3258
	BDM3Y1	0.508	0.454	0.201	3333	0.520	0.607	0.189	3248
	CDM3Y4	0.574	0.517	0.201	3334	0.570	0.669	0.189	3254
$^{8}\mathrm{B} + ^{208}\mathrm{Pb}$ $E_{lab} = 238$	M3Y-Paris	0.175	0.668	0.968	3480	0.115	0.797	1.202	3372
	M3Y-Reid	0.194	0.744	0.971	3479	0.128	0.885	1.203	3372
	B3Y-Fetal	0.241	0.931	0.972	3474	0.164	1.090	1.188	3376
	DDM3Y1	0.195	0.729	0.952	3477	0.142	0.816	1.137	3390
	BDM3Y1	0.157	0.610	0.975	3475	0.107	0.714	1.190	3375
	CDM3Y4	0.184	0.700	0.962	3477	0.131	0.795	1.158	3384

The ratios between non-halo and halo configurations, obtained for N_I (given by $\Delta \equiv N_{I-}/N_{I+}$), and for χ^2 (given by $\Sigma \equiv \chi^2_-/\chi^2_+$), for the six *nn* interactions, for the reactions $^{11}\mathrm{Be} + {}^{64}\mathrm{Zn}$ and $^{8}\mathrm{B} + {}^{120}\mathrm{Sn}$.

System	v_{nn}	Δ	Σ
$^{11}\mathrm{Be} + {}^{64}\mathrm{Zn}$	M3Y-Paris	7.880	2.214
	M3Y-Reid	7.906	2.224
	B3Y-Fetal	7.219	2.203
	DDM3Y1	7.062	2.141
	BDM3Y1	14.627	2.241
	CDM3Y4	7.442	2.154
$^{8}\mathrm{B} + {}^{120}\mathrm{Sn}$	M3Y-Paris	3.151	1.104
	M3Y-Reid	3.127	1.127
	B3Y-Fetal	2.934	1.114
	DDM3Y1	2.760	1.139
	BDM3Y1	4.967	1.062
	CDM3Y4	2.889	1.129

Conclusion

We introduce a simple optical-model approach that incorporates the ground-state structure of weakly bound nuclei via double-folding potentials. Several nucleon–nucleon interactions are tested to gauge their impact on reaction dynamics. The method is applied to elastic scattering of the halo nuclei ^{8}B and ^{11}Be off various targets, with additional calculations using non-halo configurations to isolate structural effects.

For both halo and non-halo configurations, the elastic-scattering cross sections were fitted to experimental data using standard optical model procedures, giving renormalization factors for the real and imaginary nuclear potentials, along with corresponding χ^2 values.

A comparison shows that N_I drops significantly when the halo structure is included. For the ^{11}Be+^{64}Zn, it decreases by about a factor of 8 (for M3Y-Paris, M3Y-Reid, B3Y-Fetal, CDM3Y4, and DDM3Y1), and by about 15 for BDM3Y1. The χ^2 values reduce by roughly a factor of 3 for most interactions and by about 5 for BDM3Y1.

In non-halo calculations, the larger N_I compensates for the missing halo structure by mimicking enhanced surface absorption. Including the halo, also suppresses the Coulomb-nuclear interference peak, like the effect of coupling to breakup channels. Additionally, σ_{total} is enhanced due to the halo structure, especially for the neutron-halo nucleus ^{11}Be.

This study shows that explicitly including the projectile halo in the optical model improves the accuracy of elastic scattering descriptions for weakly bound nuclei. The results highlight that accounting for this structure is essential for reliably modeling scattering observables and reaction dynamics.

Resuming notes:

- The OM is inherently one-dimensional, such that no structural properties can be directly assumed in it.
- This model does not distinguish between weakly-bound and tightly-bound nuclei.
- The effect of the missing structural properties of weakly-bound nuclei is reflected in a large multiplicative factor N_I of the folded-potential used to obtain the imaginary part of the optical potential.

Our approach to account for the g.s. in the OM:

- In weakly-bound systems, the ground-state wave function is crucial. Its extension to the periphery — due to the low breakup threshold — enhances continuum couplings and produces a static effect in breakup reactions.
- The key structural information obtained from the g.s. wave function u_0 is used to calculate the density of the weakly-bound system: $\rho(r) = \rho_c(r) + |u_0(r)|^2/(4\pi)$.
- The nuclear density together with the nuclear density of the target are used to obtained the projectile-target potential by means of the double-folding procedure. Such potential contains the ground-state structure property of the weakly-bound nucleus.

Significance:

- The origin of the suppression of the CNIP in scattering reactions induced by weakly-bound systems is not fully understood.
- The suppression of the CNIP has been explained in different ways.

  Some studies link it to couplings with breakup channels, while others attribute it to the ground-state wave function's configuration.

  For example, proton-halo systems show less suppression than neutron-halo systems because the Coulomb barrier in proton-halo systems restricts the wave function.

  Other research points to a dynamical effect from the dipole polarization potential. Regardless of the explanation, the ground-state wave function plays a key role in all cases.
- The suppression of the CNIP with the present approach suggests that the ground-state structure plays a dominant role. It offers an opportunity to investigate the interplay of static and dynamic effects in the elastic scattering.

Accounting for the exact structural geometry of weakly bound projectiles is not an incremental refinement to the Optical Model—it is a fundamental requirement for reliably describing elastic-scattering observables and nuclear reaction dynamics.

Supported by FAPESP (Proc. 2024/01533-7) and CNPq (Grant 303263/2025-3).

unesp

ECT* Nuclear Physics under the low-energy, high intensity frontier

FONDAZIONE BRUNO KESSLER

THANKS!

This work benefited greatly from discussions with **Prof. Luiz Felipe Canto**. We are deeply saddened by his loss (on June 29) and are honored to dedicate the paper to his memory.

My thanks also to the Brazilian agencies FAPESP (Proc. 2024/01533-7) and CNPq (Grant 303263/2025-3), for partial support.